Amphiregulin mediates non-cell-autonomous effect of senescence on reprogramming

Mathieu von Joest, Cheng Chen, Thibaut Douché, Jeremy Chantrel, Aurélie Chiche, Quentin Giai Gianetto, Mariette Matondo, Han Li

Cell Reports

Article

Amphiregulin mediates non-cell-autonomous effect of senescence on reprogramming

Graphical abstract

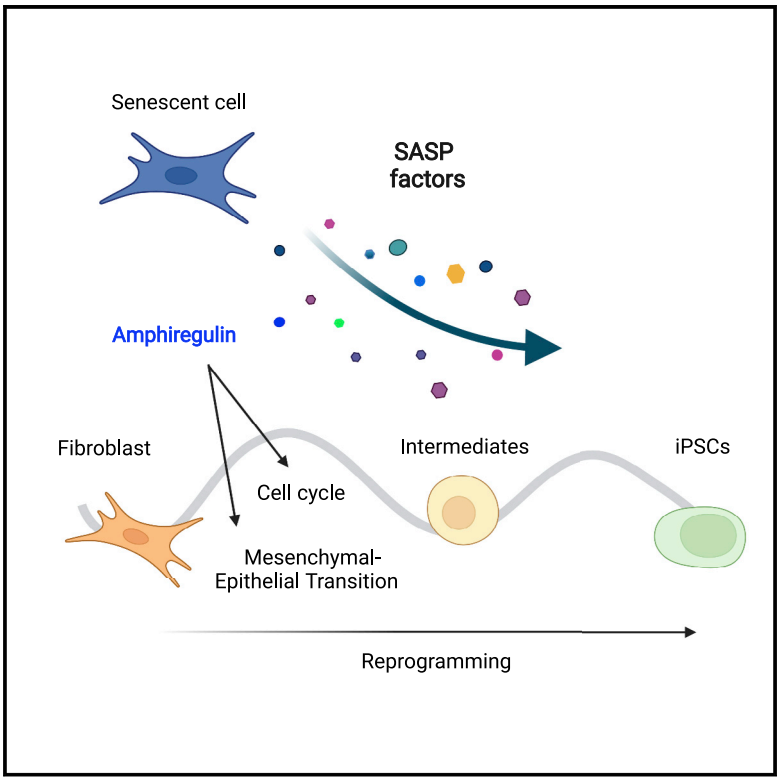

Highlights

- Paracrine senescence promotes reprogramming in a stress-dependent manner
- Quantitative proteomics identifies SASP factors facilitating reprogramming
- AREG enhances both *in vitro* and *in vivo* reprogramming
- AREG alleviates age's negative impact on *in vitro* reprogramming

Authors

Mathieu von Joest, Cheng Chen, Thibaut Douché, ..., Quentin Giai Gianetto, Mariette Matondo, Han Li

Correspondence

han.li@pasteur.fr

In brief

von Joest et al. characterize the impact of paracrine senescence on cellular reprogramming. Using quantitative proteomics, they identify a list of SASP factors that potentially facilitate cell fate conversion. Among them, amphiregulin (AREG), an EGFR ligand, promotes reprogramming both *in vitro* and *in vivo*.

von Joest et al., 2022, Cell Reports *40*, 111074
July 12, 2022
https://doi.org/10.1016/j.celrep.2022.111074

CellPress

Cell Reports

CellPress
OPEN ACCESS

Article

Amphiregulin mediates non-cell-autonomous effect of senescence on reprogramming

Mathieu von Joest,[1,5] Cheng Chen,[1] Thibaut Douché,[2] Jeremy Chantrel,[1,4] Aurélie Chiche,[1] Quentin Giai Gianetto,[2,3] Mariette Matondo,[2] and Han Li[1,6,*]

[1]Cellular Plasticity & Disease Modelling, Department of Developmental & Stem Cell Biology, CNRS UMR 3738, Institut Pasteur, 25 rue du Dr Roux, 75015 Paris, France

[2]Proteomics Platform, Mass Spectrometry for Biology Unit (MSBio), CNRS USR 2000, Institut Pasteur, 28 rue du Dr Roux, 75015 Paris, France

[3]Bioinformatics and Biostatistics Hub, Computational Biology Department, CNRS USR 3756, Institut Pasteur, 25 rue du Dr Roux, 75015 Paris, France

[4]Sorbonne Université, Collège Doctoral, 75005 Paris, France

[5]Present address: Laboratory of chromatin and gene regulation during development, Imagine Institute, INSERM UMR1163, 75015 Paris, France

[6]Lead contact

*Correspondence: han.li@pasteur.fr

https://doi.org/10.1016/j.celrep.2022.111074

SUMMARY

Cellular senescence is an irreversible growth arrest with a dynamic secretome, termed the senescence-associated secretory phenotype (SASP). Senescence is a cell-intrinsic barrier for reprogramming, whereas the SASP facilitates cell fate conversion in non-senescent cells. However, the mechanisms by which reprogramming-induced senescence regulates cell plasticity are not well understood. Here, we investigate how the heterogeneity of paracrine senescence impacts reprogramming. We show that senescence promotes *in vitro* reprogramming in a stress-dependent manner. Unbiased proteomics identifies a catalog of SASP factors involved in the cell fate conversion. Amphiregulin (AREG), frequently secreted by senescent cells, promotes *in vitro* reprogramming by accelerating proliferation and the mesenchymal-epithelial transition via EGFR signaling. AREG treatment diminishes the negative effect of donor age on reprogramming. Finally, AREG enhances *in vivo* reprogramming in skeletal muscle. Hence, various SASP factors can facilitate cellular plasticity to promote reprogramming and tissue repair.

INTRODUCTION

Cellular senescence is a stress response characterized by a permanent cell-cycle arrest, acquisition of a senescence-associated secretory phenotype (SASP), and resistance to apoptosis (Hernandez-Segura et al., 2018). Senescence is involved in a variety of biological and pathological processes, including development, tissue repair, tumorigenesis, and organism aging (Munoz-Espin and Serrano, 2014; Rhinn et al., 2019). Of note, SASP plays a crucial role in mediating senescence non-cell-autonomous functions by interacting with neighboring cells and the surrounding microenvironment (Ito et al., 2017). It is becoming clear that senescence phenotypes, particularly of SASP composition, are highly heterogeneous and depend on the initial stimuli, the affected cell type, and the anatomic location (Hernandez-Segura et al., 2017; Ito et al., 2017).

Cellular reprogramming is a process of converting fully differentiated cells back to the pluripotent state, which has tremendous potentials in many areas of biomedical research (Takahashi and Yamanaka, 2006; Robinton and Daley, 2012). Interestingly, recent studies revealed that senescence has both cell-autonomous and non-cell-autonomous effects on reprogramming (Aarts et al., 2017; Banito et al., 2009; Chiche et al., 2017; Mosteiro et al., 2016, 2018). Ectopic expression of reprogramming factors Oct4, Klf4, Sox2, and c-Myc (OSKM) induced senescence as a cell-intrinsic barrier for reprogramming (Banito et al., 2009), which in turn promotes cellular plasticity and reprogramming in the non-senescent cells via SASP, in particular by interleukin-6 (IL-6) (Chiche et al., 2017; Mosteiro et al., 2016, 2018). However, the mechanisms by which paracrine senescence, with specific SASP factor(s), regulate cellular plasticity in the context of reprogramming remain not fully understood.

The epidermal growth factor receptor (EGFR) signaling pathway is one of the most important pathways that regulate cellular growth, proliferation, differentiation, and survival (Herbst, 2004). Although it is important for embryonic stem cells to function (Schuldiner et al., 2000; Yu et al., 2019) and for early embryonic development (Kim et al., 1999), the role of the EGFR signaling pathway in somatic reprogramming remains poorly understood. A variety of senescent cells produce abundant amphiregulin (AREG) (Coppe et al., 2010), a low-affinity EGFR ligand (Jones et al., 1999; Shoyab et al., 1988). Of note, accumulating evidence indicates that AREG is a vital mediator of the immune response in infection and tissue repair (Zaiss et al., 2015). It has been suggested that AREG regulates senescence (Pommer

et al., 2021) and contributes to an immunosuppressive tumor microenvironment (Xu et al., 2019). Given the pleiotropic functions of AREG, its roles in mediating senescence functions remain largely unexplored.

In this study, we investigated how paracrine senescence impacts reprogramming focusing on the stress-dependent SASP heterogeneity and identified a collection of SASP factors potentially important for cellular plasticity using unbiased proteomic analysis. Next, we demonstrated that AREG enhances reprogramming both *in vitro* and *in vivo* via EGFR and alleviates the age-associated reduction in reprogramming.

RESULTS

Paracrine senescence promotes *in vitro* reprogramming in a stress-dependent manner

Given that senescence can impact reprogramming in both a cell-autonomous and a non-cell-autonomous manner (Chiche et al., 2020), SASP composition is highly context dependent as determined by both the initial stress and the tissue/cell of origin (Hernandez-Segura et al., 2017; Ito et al., 2017). We reasoned that stress-dependent SASP might impact reprogramming efficiency differently. To address this question, we treated non-reprogrammable wild-type (WT) primary mouse embryonic fibroblasts (MEFs) with three different stimuli (replicative senescence [RS], γ-irradiation [IRIS], and oncogene-induced senescence [OIS]) to induce senescence (Figures S1A and S1B). Meanwhile, we used the MEFs generated from a previously established reprogrammable mouse model (i4F) (Abad et al., 2013). The reprogramming was induced by adding doxycycline (DOX) in i4F-MEFs either co-cultured with the senescent WT MEFs (co-culture) or cultured directly with the senescence-conditioned medium (CM) according to the experimental scheme illustrated (Figure 1A). After 12 days of DOX treatment, induced pluripotent stem cell (iPSC) colonies were stained using alkaline phosphatase to determine the reprogramming efficiency. For the co-culture system, i4F MEFs were seeded on top of 2×10^5 WT MEFs (either control or OIS treated) with various ratios (1:3, 1:5, and 1:10 [i4F:WT]), to determine the optimal experimental condition. We found that the reprogramming efficiency increased most at a ratio of 1:10 (i4F:WT) (Figure S1C). Next, we compared the relative reprogramming efficiency of i4F MEFs and found that in both systems all stimuli can increase reprogramming efficiency ranging from RS as the least to OIS as the most, except that the positive effect of RS is diminished in the CM system (Figures 1B and 1C).

Reprogramming is a stepwise process with distinct phases: initiation, maturation, and stabilization (Samavarchi-Tehrani et al., 2010). To determine at which stage the SASP exposure is most important for enhancing reprogramming, we cultured i4F with either OIS-CM or Ctrl-CM in different orders (Figures 1D and S1D). Culturing i4F-MEFs with OIS-CM for the first 3 days was sufficient to induce the highest fold increase in reprogramming (Figure 1D). Conversely, initiating reprogramming with Ctrl-CM for 3 days and replacing this with OIS-CM completely abolished the beneficial effect (Figure S1D). Active cell proliferation is rate limiting for successful reprogramming (Ruiz et al., 2011), and senescent cells secrete various growth factors (Coppe et al., 2010). Therefore, we compared the growth properties of i4F MEFs cultured with either OIS-CM or Ctrl-CM over 12 days in the absence of DOX. The bromodeoxyuridine (BrdU) incorporation rates after 72 h were similar between Ctrl and OIS (Figure S1E). However, the accumulative growth curve indicated that i4F MEFs grew faster in OIS-CM than in Ctrl-CM (Figure S1F). Hence, certain SASP factors promote *in vitro* reprogramming transiently at the initiation phase of reprogramming, which partially correlates with an enhanced proliferation rate.

Conditioned medium of OIS-Il6$^{-/-}$ promoted reprogramming efficiently

We sought to identify SASP factors responsible for the stress-dependent effect on reprogramming. Given that IL-6 signaling is required for *in vitro* reprogramming (Brady et al., 2013; Mai et al., 2018), and that IL-6 is a crucial mediator of the senescence paracrine signals in promoting *in vivo* reprogramming (Chiche et al., 2017; Mosteiro et al., 2016, 2018), we determined firstly the effect of CM of senescent MEFs derived from *Il6*$^{-/-}$ mice on reprogramming. Of note, IL-6 plays a critical role in mediating OIS, and reduction of IL-6 via RNA interference efficiently bypassed OIS in human diploid fibroblasts (Kuilman et al., 2008). Interestingly, we found that *Il6*$^{-/-}$ MEF entered senescence efficiently upon OIS in 20% and 3% oxygen, judging by both proliferation (Figure S2A) and qPCR (Figure S2B). Surprisingly, CM generated from senescent *Il6*$^{-/-}$ MEFs by IRIS or OIS enhanced reprogramming efficiency to a similar level as WT (Figure 2A). To ensure that the observed enhancement is IL-6 independent, we compared the IL-6 level in the cell lysate and medium (secreted) of both WT and *Il6*$^{-/-}$ upon OIS by ELISA. In WT, IL-6 is significantly increased in both cell lysate and medium upon OIS. Interestingly, IL-6 is increased in the cell lysate but non-detectable in *Il6*$^{-/-}$ MEFs medium upon OIS (Figure S2C), suggesting a defective secretion of IL-6 in *Il6*$^{-/-}$ MEFs. Furthermore, IL-6 neutralizing antibody could potently repress the increased reprogramming efficiency only in the CM-WT but failed to do so in the CM-*Il6*$^{-/-}$ (Figures 2B and S2D). Thus, there are SASP factors other than IL-6 that can robustly promote *in vitro* reprogramming.

In vivo reprogramming in the skeletal muscle is not affected by IL-6 deficiency

We reported previously that injury-induced senescence enabled reprogramming in the skeletal muscle (Chiche et al., 2017). We wondered whether tissue injury could induce reprogramming in the skeletal muscle of *Il6*$^{-/-}$ mice. To test this, we generated an *Il6*$^{-/-}$;i4F mouse model and injured the tibialis anterior (TA) muscle of both *Il6*$^{+/-}$;i4F and *Il6*$^{-/-}$;i4F mice with snake venom cardiotoxin (CTX). At the same time, we added DOX to the drinking water for 7 days to induce *in vivo* reprogramming and TAs were collected at 10 days post-injury (dpi) as described previously (Chiche et al., 2017). The expression of the OSKM triggered extensive dysplasia and reprogramming (Nanog$^+$ cells) in the injured TA of male i4F mice (Figures 2C and S2E). Consistent with a previous report (Mosteiro et al., 2018), the reprogramming was significantly reduced in female i4F mice compared with male i4F mice (Figures 2C, 2D, and S2E), which could be attributed to the anti-inflammatory effect of estrogens.

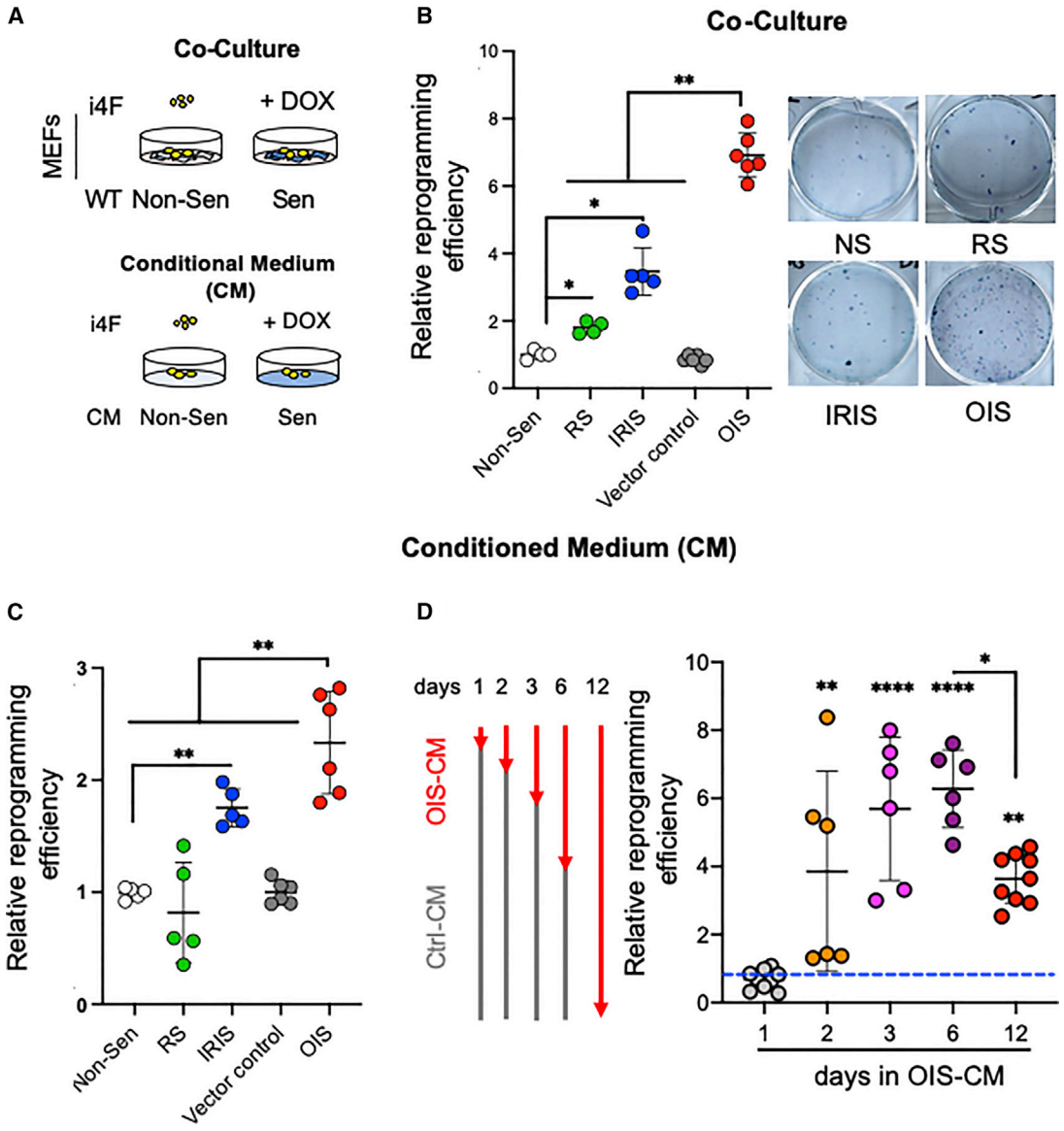

Figure 1. Senescence promotes *in vitro* reprogramming in a stress-dependent manner

(A) Scheme of the experiments.

(B and C) Relative *in vitro* reprogramming efficiency of i4F MEFs exposed to secretome of non-senescent compared with senescent cells generated by different stress (corresponding to the respective controls: RS and IRIS to non-sen and OIS to vector alone). RS, replicative senescence; IRIS, γ-irradiation; OIS, oncogene-induced senescence. (B) Co-culture system. Representative image of plate stained with alkaline phosphatase (AP) to reveal colonies arising from reprogramming (right panel). (C) Conditioned medium (CM) system.

(D) Reprogramming fold change of i4F MEFs cultured in different duration of OIS-CM before switching to Ctrl-CM. Scheme of the experiment (left panel). All the reprogramming fold changes was normalized to i4F in Ctrl-CM for 12 days, indicated by the blue dash line. Data correspond to the average ±SD from three independent experiments using i4F MEFs from two different embryos for every experiment (B–D). Statistical significance was assessed by ordinary one-way ANOVA test: *p < 0.05, **p < 0.01, ****p < 0.0001. See also Figure S1.

Interestingly, *Il6*$^{-/-}$; i4F mice exhibited a similar level of dysplasia and Nanog^{+} cells as the sex-matched *Il6*$^{+/-}$;i4F mice (Figures 2C, 2D, and S2E). Besides, we did not observe a difference in the senescence induction in males regardless of the genotype (Figures S2F and S2G). Thus, *in vivo* reprogramming in the skeletal muscle is not impaired in the IL-6-deficient reprogrammable mice.

Soluble factor fraction of the CM-OIS mediates *in vitro* reprogramming

To gain a comprehensive profile of the heterogeneous composition of SASP, we determined firstly the effect of different fractions of CM on reprogramming, which could facilitate reprogramming due to secreted proteins, extracellular vesicles, or small-molecule metabolites. We examined whether the boiled

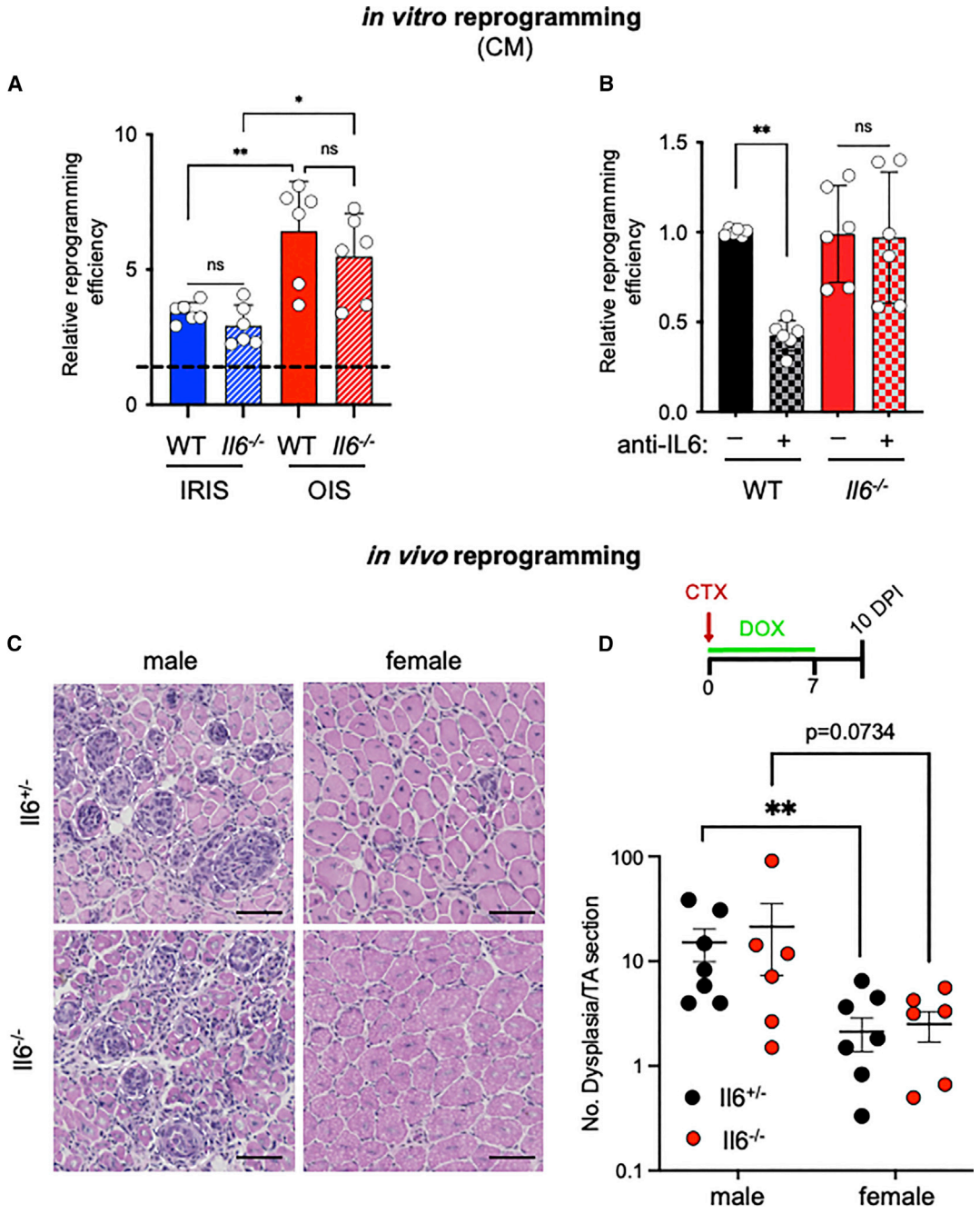

Figure 2. *In vivo* reprogramming in the skeletal muscle occurs normally in *Il6*$^{-/-}$ mice

(A) Relative reprogramming efficiency of the i4F MEFs cultured in the CM derived from either WT or *Il6*$^{-/-}$ senescent cells. Senescence was induced using two different stresses, IRIS and OIS. Fold change was normalized with CM derived of respective non-senescent counterparts.

(B) Reprogramming efficiency of i4F MEFs cultured in CM of WT or *Il6*$^{-/-}$ senescent cells compared with treatment of IL-6 blocking antibody. Senescence was induced by overexpression of oncogene (OIS). Data correspond to the average ± SD from three independent experiments using i4F MEFs from two different embryos for every experiment (A and B).

(C) Transverse TA cryosections of indicated genotypes and sex after histological staining with hematoxylin and eosin (H&E). Dashed circle highlights dysplasia region. Scale bar, 100 μm.

(D) Experimental scheme (upper panel) and quantification of (C). Data correspond to the average ±SD of using at least six mice per group (average of two TA per mouse). Statistical significance was assessed by ordinary one-way ANOVA test: *p < 0.05, **p < 0.01, ***p < 0.001. See also Figure S2.

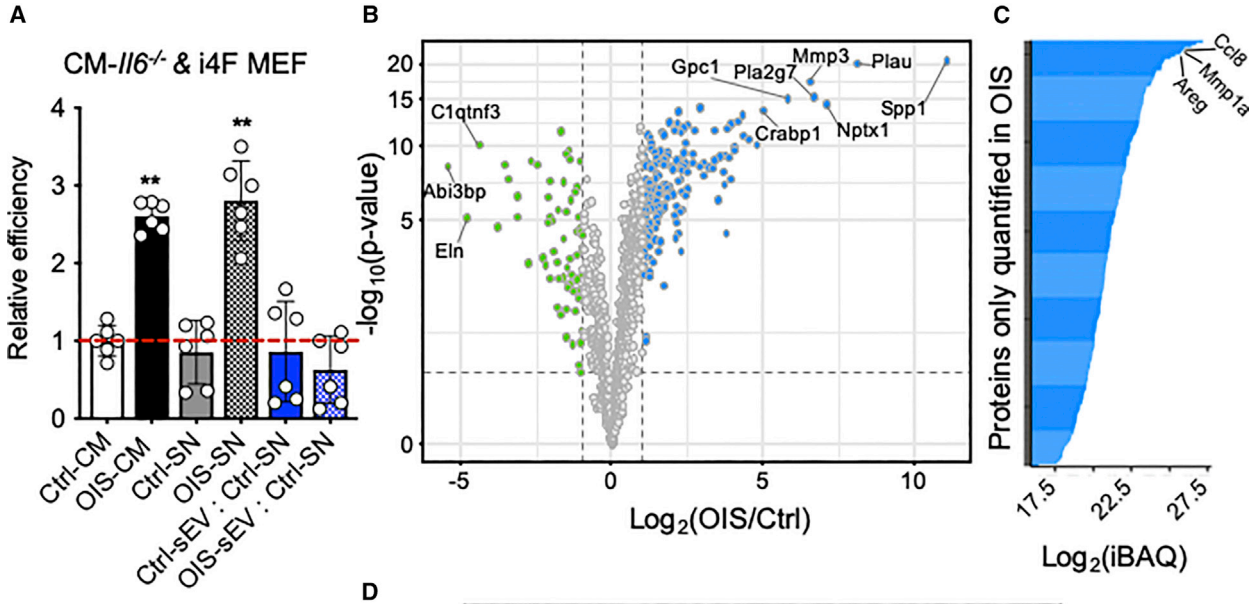

D

Total identified: 1955			
OIS>Ctrl	OIS Only	Ctrl>OIS	Ctrl Only
170	185	67	32

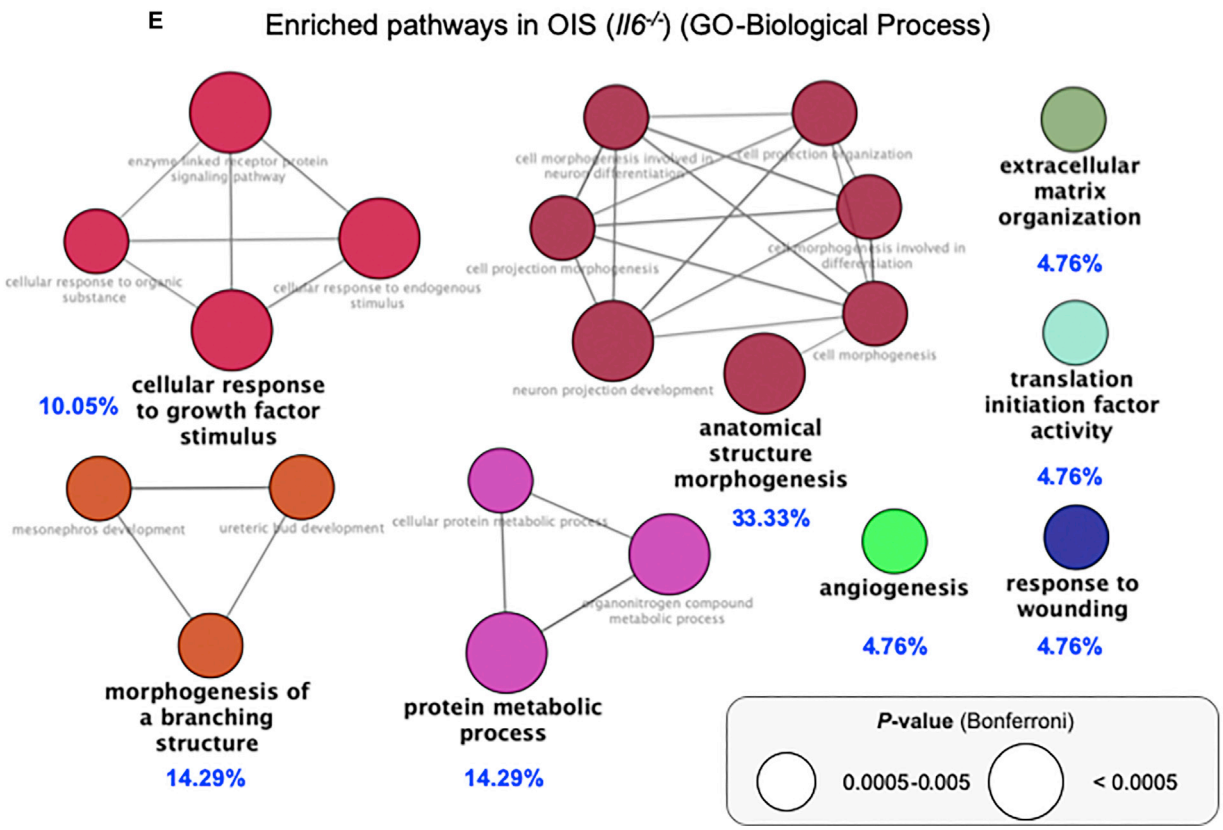

(legend on next page)

CM could promote *in vitro* reprogramming since boiling denatures most proteins without affecting small-molecule metabolites, and found that boiled CM completely abolished *in vitro* reprogramming, indicating that secreted proteins are crucial in promoting reprogramming (Figure S3A).

Exosomes are small extracellular vesicles (sEV) released from almost all cell types and are critical mediators of intercellular communication (Kalluri and LeBleu, 2020). Increasing evidence suggests that senescent cells secret exosomes with distinct features, contributing to paracrine senescence (Borghesan et al., 2019). To examine whether senescence-associated exosomes regulate *in vitro* reprogramming, we isolated sEV and supernatant (SN) fractions from Ctrl-CM and OIS-CM using serial ultracentrifugation and filtering with a 0.22-μm filter (Thery et al., 2006). Both OIS-sEV and Ctrl-sEV were suspended in Ctrl-SN to determine whether they can drive paracrine senescence. Consistent with the previous report (Borghesan et al., 2019), the OIS-sEV in Ctrl-SN induces several senescence markers in i4F MEFs, as shown by a decrease in BrdU incorporation and an increase in mRNA expression of p16 and ARF (Figures S3B and S3C). Next, we wondered whether OIS-sEV could also affect reprogramming. Compared with Ctrl-SN, the OIS-SN significantly enhanced the reprogramming efficiency to a similar level as OIS-CM (Figure 3A). However, OIS-sEV in Ctrl-SN exhibited a much lower reprogramming efficiency than OIS-SN, similarly to Ctrl-sEV in Ctrl-SN (Figure 3A). Hence, the soluble fraction of OIS-CM is essential for promoting *in vitro* reprogramming.

Quantitative proteomics analysis of SASP composition

Next, we set to determine the SASP composition in the soluble fraction of OIS-CM. To maximize the detection of SASP factors important for reprogramming other than IL-6, we isolated the soluble protein fractions from the OIS-CM and Ctrl-CM of *Il6*$^{-/-}$ MEFs to perform a label-free quantitative proteomic analysis (Gillet et al., 2012). A stringent list of SASP proteins was generated by selecting proteins identified and quantified only in the six replicates of at least one condition (Figure S3D). The proteomic analysis identified a total of 1,955 proteins in both conditions, including 249 proteins with a significant differential expression ($q < 0.01$) that had a change of at least 2-fold (OIS/CTL) (Figure 3B). Of note, 217 proteins were exclusively detected in one condition (185 in OIS and 32 in Ctrl) (Figure 3D), which were included in the data analysis. Relative protein quantification and statistical details are presented in Table S1. We found many known SASP factors more abundantly secreted in the OIS-SN, such as SPP1, PLAU, and MMP3 (Figure S3E). Of note, we did not detect IL-6 in either condition. Interestingly, there is less than 50% overlap between our study and a recent large-scale human SASP proteomic study (human fibroblast-OIS, 115/355) (Table S2) (Basisty et al., 2020), suggesting that they are heterogeneous in SASP composition between species (Hernandez-Segura et al., 2017).

To identify which biological pathways/responses are mediated by SASP factors, we performed pathway and network analyses on the proteins that are either more abundantly or exclusively secreted from the OIS condition. We found that the most dominant clusters of gene ontology pathways are related to morphogenesis and stress response, including cell morphogenesis in development and differentiation, response to growth factor, wounding response, and angiogenesis (Figure 3E; Table S3). Besides, hallmark gene set enrichment analysis (GSEA) revealed several pathways that are associated with paracrine senescence and somatic reprogramming, including epithelial-to-mesenchymal transition (EMT) (Ansieau et al., 2008; Liu et al., 2013) and the p53 pathway (Coppe et al., 2010; Hong et al., 2009; Kawamura et al., 2009; Marion et al., 2009; Utikal et al., 2009) (Figure S3F).

AREG enhances *in vitro* reprogramming efficiency and kinetics

Notably, we found that AREG, an EGFR ligand (Shoyab et al., 1989), is one of the most abundant proteins exclusively expressed under OIS conditions (Figures 3C, S4A; Table S3). AREG has diverse functions in development, tissue regeneration, and tumorigenesis (Zaiss et al., 2015). Although AREG is strongly induced in senescent cells by various stresses (Pommer et al., 2021), its functional relevance in paracrine senescence remains largely unexplored. Of note, AREG is also induced upon muscle injury and has been reported to play an important role during muscle regeneration, which is particularly relevant to our *in vivo* reprogramming system (Burzyn et al., 2013; Chiche et al., 2017). Therefore, we wondered whether AREG could partially mediate the effect of paracrine senescence on reprogramming both *in vitro* and *in vivo*. Interestingly, AREG is the only EGFR ligand that has significantly increased mRNA expression in OIS compared with IRIS (Figure S4B). To formally test the effect of AREG on reprogramming, we added different concentrations of the recombinant AREG protein for the first 3 days during reprogramming, consistent with the CM experiment (Figure 1D). AREG treatment enhanced reprogramming efficiency in a dosage-dependent manner (Figure 4A). Next, we removed DOX at different time points to examine the ability of AREG to

Figure 3. Proteomic analysis of oncogenic stress-induced secretome in *Il6*$^{-/-}$ MEFs

(A) Fold change of reprogramming efficiency of i4F MEFs cultured in indicated different combination of various fractions of CM from non-senescent (Ctrl) or senescent (OIS) *Il6*$^{-/-}$. SN, supernatants (soluble proteins); sEV, small extracellular vesicles (exosome). Reprogramming efficiency fold change normalized to Ctrl-CM. Data correspond to the average ±SD from three independent experiments using i4F MEFs generated from two different embryos for every experiment.

(B) Volcano plot shows $\log_2$ fold change (FC) in protein intensity against the –log10 p value in SEN compared with Ctrl; blue dots are proteins with significant differential expression (FDR 1% and >2-FC).

(C) The intensity of proteins only quantified in OIS (Table S1). Protein intensity was measured by the total intensities divided by the identified peptides for one protein (iBAQ).

(D) Summary of proteins either with significantly altered secretion ($q < 0.01$ and >2-FC) by senescent (OIS) compared with quiescent cells (Ctrl), or exclusively detected in all repeats from one condition, following oncogenic stress (OIS) in senescent *Il6*$^{-/-}$ primary MEFs (Table S1).

(E) ClueGO (Bindea et al., 2009) pathway enrichment and network analyses of the OIS secretome. Pathways of the same color have ≥50% similarity. Connecting lines represent Kappa connectivity scores >40%. Statistical significance was assessed by ordinary one-way ANOVA test: $^{**}p < 0.01$. See also Figure S3.

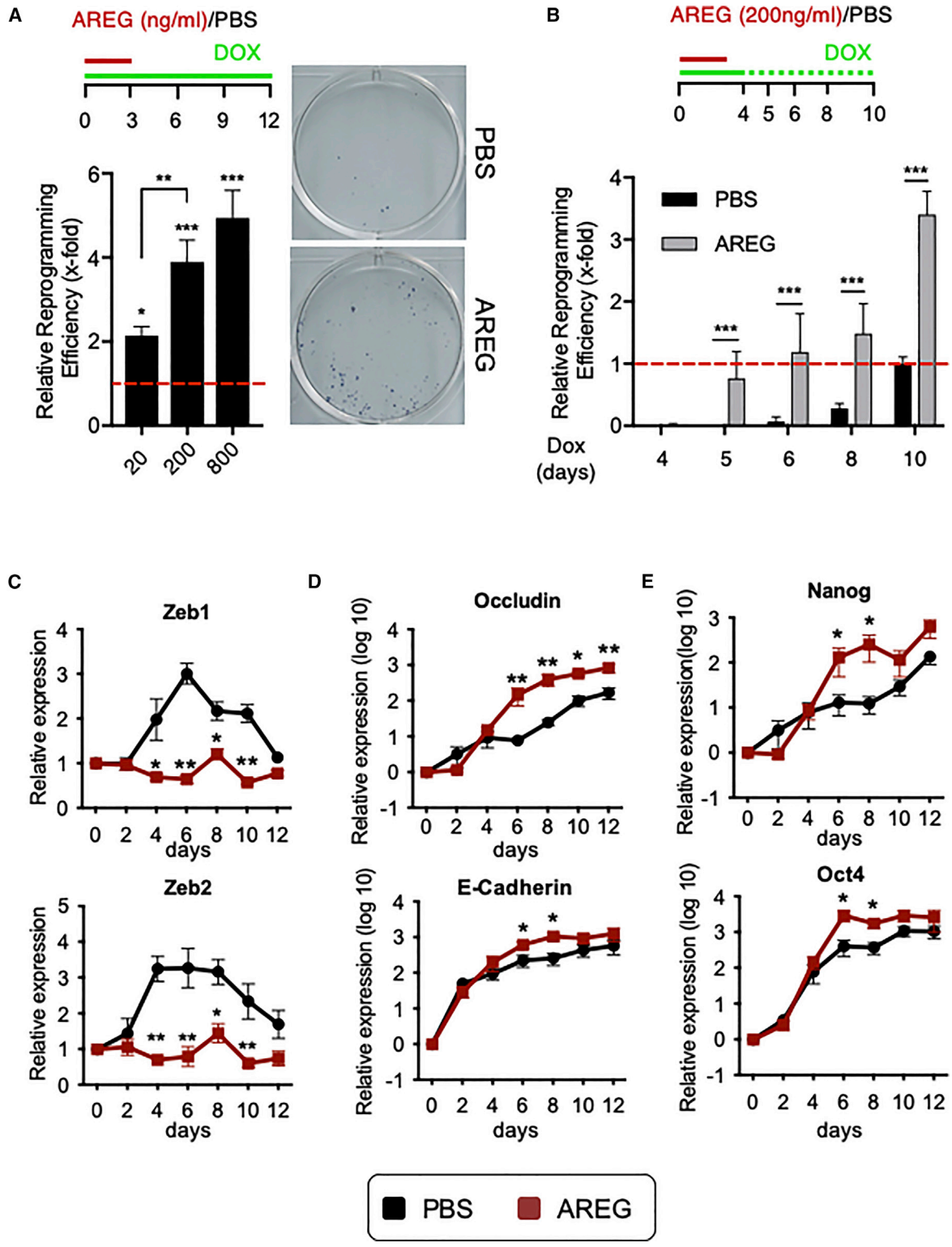

Figure 4. AREG promotes *in vitro* reprogramming

(A) Experimental scheme (upper panel). Fold change of reprogramming efficiency of i4F MEFs with different dosages of recombinant AREG protein. Normalized to vehicle control (PBS). Representative image of plate stained with alkaline phosphatase (AP) to reveal colonies arising from reprogramming (right panel).

(B) Experimental scheme (upper panel). Comparison of reprogramming efficiency between PBS and recombinant AREG after different duration of DOX treatment. Data correspond to the average ±SD from three independent experiments using i4F MEFs generated from two different embryos for every experiment (A and B).

(legend continued on next page)

facilitate OSKM transgene-independent clonal growth, a hallmark of iPSCs. AREG treatment yielded iPSC clones after only 5 days of OSKM expression, compared with 8 days under the control conditions (Figure 4B), suggesting a faster reprogramming kinetic.

AREG accelerates cell cycle and the process of MET during reprogramming

We sought to understand the mechanism by which AREG promotes reprogramming. The reported role of AREG in proliferation and EMT (Berasain and Avila, 2014) prompted us to analyze cell proliferation and the mesenchymal-epithelial transition (MET) process, two important cellular events that occurred in the early stage of reprogramming (Sancho-Martinez and Izpisua Belmonte, 2013). AREG treatment led to a larger fraction of cells in S-phase and increased cell proliferation globally in MEFs alone (Figures S4C and S4D). Next, we checked whether AREG could affect the MET process during reprogramming. We measured the expression of several mesenchymal and epithelial cell markers at different time points throughout reprogramming by qPCR. In the control, the expression of the mesenchymal markers, Zeb1 and Zeb2, were transiently upregulated and gradually suppressed afterward. These markers were suppressed throughout the reprogramming process in the AREG-treated condition (Figure 4C). Conversely, the expression of the epithelial markers, Occludin and E-Cadherin, was higher in samples treated with AREG than in control (Figure 4D). Besides, the expression of all the pluripotency markers, endogenous Oct4, Sox2, Klf4, Nanog, Lin28, and Esrrb, gradually increased and peaked at the last stage of reprogramming in control. However, under AREG-treated conditions, endogenous Oct4 and Nanog expression sharply increased at 6 days and reached a plateau earlier than in controls (Figure 4E). However, the expression dynamic of other pluripotent markers remained the same (Figure S4E), suggesting an action upon Nanog and Oct4 specifically rather than a mere reflection of the accelerated reprogramming. These results indicate that AREG enhances the efficiency and kinetic of reprogramming by increasing proliferation rates and potentially facilitating the MET process.

EGFR signaling pathway is important for reprogramming

Since AREG is an atypical EGFR ligand (Zaiss et al., 2015), we wondered whether other EGFR ligands could also promote somatic reprogramming and found that additional EGF also improved the reprogramming efficiency (Figure 5A). Next, we examined whether EGFR activation is necessary for the enhancement. AREG and DOX combination strongly induced the activation of EGFR compared with DOX alone or untreated control determined by the level of the phosphorylated EGFR using western blotting (Figure S5A). Besides, Lapatinib, a dual tyrosine kinase inhibitor of EGFR and human epidermal growth factor receptor-2 (HER2) (Wood et al., 2004), canceled the effect of AREG on reprogramming (Figures 5B and S5A). Of note, a high concentration of Lapatinib alone significantly repressed reprogramming (Figure S5B), suggesting that the EGFR signaling pathway might be required for reprogramming. Finally, AREG treatment also enhanced the reprogramming efficient of human fibroblasts, BJ cells (Figure 5C).

AREG rescues age-dependent reduction in reprogramming

Previously, we reported that murine dermal fibroblasts (MDFs) derived from old (>2 years) mice had a significant reduction in reprogramming efficiency compared with MDFs derived from young (2 months) mice (Li et al., 2009). Because AREG induces cell proliferation, we investigated whether AREG can improve reprogramming in this context. Consistent with the previous report, MDFs from old (>2 years) i4F mice had much lower reprogramming efficiency compared with MDFs from young (2 months) i4F mice (Figure 5D). Notably, the addition of AREG to the aged MDFs rescued their low reprogramming efficiency to the same level as the young MDFs (Figure 5D).

AREG promotes *in vivo* reprogramming in the skeletal muscle

It has been reported that AREG enhances the myogenic differentiation of skeletal muscle stem cells (MuSCs) *in vitro* and facilitates muscle regeneration (Burzyn et al., 2013). We previously reported that MuSC is a cell of origin for *in vivo* reprogramming (Chiche et al., 2017). Therefore, we hypothesize that AREG might also improve *in vivo* reprogramming in the injured muscle. To address this question, we administered AREG to the CTX-injured, DOX-treated male i4F mice according to the experimental scheme illustrated (Figure 5E) and evaluated reprogramming and senescence induction at 10 dpi. (Note that the initial AREG injection was done intramuscularly, as described previously [Burzyn et al., 2013].) There were many more Nanog$^+$ cells in the TA sections from mice treated with AREG than in the control group (Figures 5F and 5G). Conversely, there is no apparent difference in senescence induction detected by SAβGal staining (Figures 5F and 5G). Interestingly, we also observed more Nanog$^+$ cells in both pancreas and kidney but not in the liver (Figure S5C), suggesting a tissue-specific effect of AREG on *in vivo* reprogramming.

DISCUSSION

Here, we report that the impact of paracrine senescence on reprogramming is stress dependent. The quantitative proteomic analysis on the senescence-associated secretome identified a catalog of factors involved in various biological processes that could potentially impact cell plasticity. We demonstrated that the AREG enhances *in vitro* reprogramming efficiency and kinetics, at least in part by accelerating somatic cell proliferation and the process of MET. Of note, AREG treatment rescues the

(C–E) Kinetics of expression of indicated genes at the indicated days during reprogramming compared between PBS and AREG as measured by qRT-PCR. Data correspond to the average ± SEM from three independent experiments using i4F MEFs generated from two different embryos for every experiment. For every assay, qRT-PCR values were obtained in duplicate. Statistical significance was assessed by ordinary one-way ANOVA test for (A), and two-way ANOVA test for (B–E): *$p < 0.05$, **$p < 0.01$, ***$p < 0.001$. See also Figure S4.

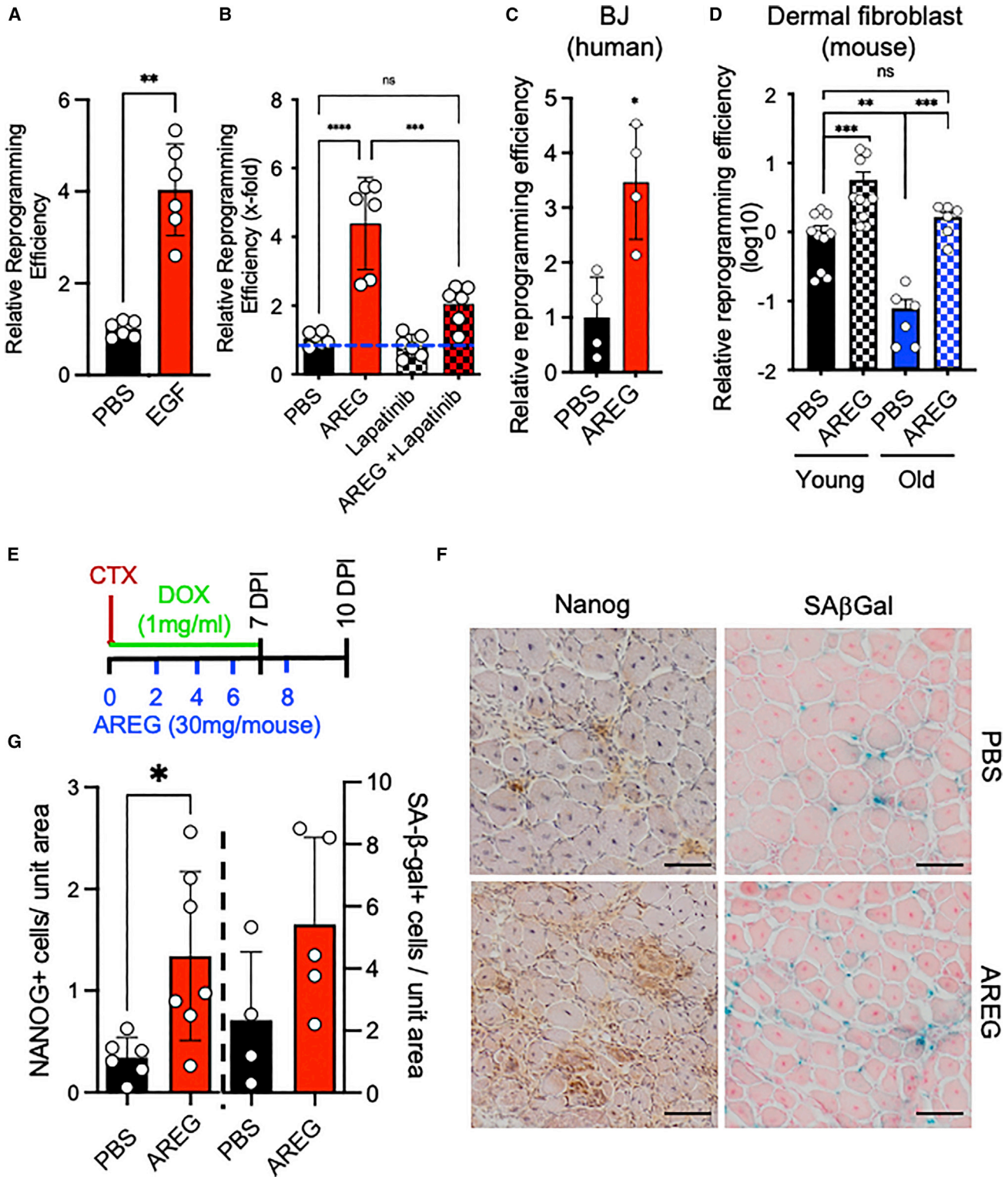

Figure 5. AREG promotes *in vivo* reprogramming

(A) Relative reprogramming efficiency of i4F MEFs treated with EGF (100 ng/mL). Relative to PBS-treated sample.

(B) Relative reprogramming efficiency of i4F MEFs with indicated treatment. Relative to the PBS-treated sample. Data correspond to the average ±SD from three independent experiments using i4F MEFs generated from two different embryos for every experiment (A and B).

(legend continued on next page)

age-associated reduction in reprogramming and facilitate *in vivo* reprogramming in the skeletal muscle.

IL-6 is required for OIS (Kuilman et al., 2008). Surprisingly, we could efficiently induce senescence in *Il6*$^{-/-}$ MEFs under 20% and 3% oxygen conditions (Figures S2A and S2B) (Kopf et al., 1994). Notably, we detected increased IL-6 in the cell lysate but not in the OIS-*Il6*$^{-/-}$ medium by ELISA (Figure S2C). Therefore, we speculate that the *Il6*$^{-/-}$ model used in this study is not a complete knockout but a specific defect in IL-6 secretion, similar to a functional knockout mouse model. Thus, the cell-intrinsic role of IL-6 on OIS might be intact in *Il6*$^{-/-}$ MEFs.

A recent study reported a reduction of reprogramming in the pancreas of i4F;*Il6*$^{-/-}$ mice (Mosteiro et al., 2018), whereas we found that the *in vivo* reprogramming in the muscle is not affected in the *Il6*$^{-/-}$ mice (Figures 2C and 2D). Firstly, reprogramming-induced and injury-induced senescence might produce different SASP factors (Chiche et al., 2017; Mosteiro et al., 2018). Besides, although IL-6 is a myokine vital for muscle formation and growth (Serrano et al., 2008), muscle regeneration is only mildly affected in *Il6*$^{-/-}$ mice (Zhang et al., 2013), suggesting a potential compensation by other members of the IL-6 cytokine family. Therefore, the tissue-specific requirement of IL-6 for *in vivo* reprogramming might be due to a distinct stress/tissue-dependent senescence secretome and the pleiotropic functions of IL-6.

The role of the EGFR pathway during somatic reprogramming remains largely elusive. We found that both AREG and EGF could enhance reprogramming efficiency (Figures 4A, 4B, and 5A), most likely in an EGFR-dependent manner. Specifically, AREG could accelerate cell proliferation (Figure S4C) and suppress mesenchymal markers (Figure 4C), suggesting that the AREG/EGFR pathway might affect several cellular events necessary for the initiation phase of reprogramming (Sancho-Martinez and Izpisua Belmonte, 2013). Interestingly, AREG could alleviate age's negative impact on reprogramming (Figure 5B), providing a straightforward solution to improve iPSC generation during aging (Mahmoudi et al., 2019). Of note, AREG treatment failed to further enhance reprogramming to a similar level as in the young (Figure 5D), reflecting the attenuated EGFR signaling in the aged skin fibroblasts as reported previously (Shiraha et al., 2000; Tran et al., 2003).

It has been reported that AREG could facilitate the differentiation of MuSCs *in vitro* (Burzyn et al., 2013; Zaiss et al., 2015). Therefore, AREG might directly promote the cell plasticity of MuSCs, a primary cell origin of reprogramming in the muscle (Chiche et al., 2017). In addition, we observed that AREG promotes reprogramming in a tissue-specific manner (Figure S5C), which might reflect the distinct requirement of different cell origins for reprogramming. Of note, recent studies showed that cyclic expression of OSKM could enhance tissue regeneration (Ocampo et al., 2016). Given that senescence is important for optimal wound healing (Demaria et al., 2014) and limb regeneration (Yun et al., 2015), future investigation is warranted to determine whether the rejuvenation effect of partial reprogramming is partially mediated by senescence.

In summary, we dissected the impact of paracrine senescence on reprogramming and revealed the role of the AREG-EGFR signaling pathway in reprogramming. These findings may have important implications for understanding senescence's involvement in tissue repair and *in vivo* reprogramming.

Limitations of the study

We used OIS-MEFs to proxy for senescence induced by OSKM overexpression or muscle injury. However, the SASP is highly cell type and stress dependent and we have a limited understanding of the landscape of *in vivo* senescence, including the senescent cell types. Therefore, this study does not fully recapitulate the *in vivo* scenario. Besides, the cell origin of *in vivo* reprogramming in most tissues is largely unknown. The tissue-specific requirement of certain SASP factors for *in vivo* reprogramming is not explored in this study. Future investigation should further elucidate the context-dependent SASP heterogeneity and its impact on *in vivo* reprogramming in a tissue-specific manner. Finally, the HER2 involvement in AREG-dependent reprogramming enhancement is not investigated.

STAR★METHODS

Detailed methods are provided in the online version of this paper and include the following:

- KEY RESOURCES TABLE
- RESOURCE AVAILABILITY
  - Lead contact
  - Materials availability
  - Data and code availability
- EXPERIMENTAL MODELS AND SUBJECT DETAILS
  - Mice and breeding
- METHOD DETAILS
  - Animal procedures
  - Cell culture conditions
  - Induction of senescence
  - Collection of CM
  - Soluble fraction and sEV isolation
  - *In vitro* reprogramming in co-culture & CM system
  - Plasmids and infections
  - Proteomic sample preparation
- QUANTIFICATION AND STATISTICAL ANALYSIS

(C) Relative reprogramming efficiency of human BJ cells treated with human AREG (200 ng/mL). Relative to the PBS-treated sample. Data correspond to the average ± SD from four independent experiments with triplicates for every experiment.
(D) Reprogramming efficiency of dermal fibroblasts derived from i4F mice with the indicated treatment and age. Data correspond to the average ±SD from three independent experiments using MDF isolates from at least two mice.
(E) Experimental scheme for AREG administration during *in vivo* reprogramming.
(F) Representative TA sections with immunohistochemistry staining of anti-Nanog and histological staining of SAβGal of indicated treatment. Scale bar, 100 μm.
(G) Quantification of (E). Data correspond to the average ±SD of using at least five mice per treatment (average of two TA per mouse). Statistical significance was assessed by the Mann-Whitney test (A) and ordinary one-way ANOVA (B, C, and F): *p < 0.05, **p < 0.01, ***p < 0.001. See also Figure S5.

SUPPLEMENTAL INFORMATION

Supplemental information can be found online at https://doi.org/10.1016/j.celrep.2022.111074.

ACKNOWLEDGMENTS

We are indebted to Jun Zhang for his excellent technical support in image analysis. We are grateful to the Central Animal Facility, the Proteomic Platform, the Cytometry Platform, and the Bioinformatics and Biostatistics Hub of the Institut Pasteur.Work in the laboratory of H.L. is funded by Institut Pasteur, Centre National pour la Recherche Scientific, and the Agence Nationale de la Recherche, France (Laboratoire d'Excellence Revive, Investissement d'Avenir; ANR-10-LABX-73; ANR-16-CE13-0017; ANR-21-CE13-0006-01). A.C. was funded by the postdoctoral fellowships from the Revive Consortium.

AUTHOR CONTRIBUTIONS

M.v.J. performed most of the experimental work, contributed to experimental design, data analysis, and discussions. C.C. made critical experimental contributions. J.C. and A.C. contributed experimentally. T.D. performed proteomic analysis and data acquisition. Q.G.G. performed statistical and bioinformatic analysis. M.M. supervised the proteomic analysis and data interpretation. H.L. supervised the study, designed the experimental plan, interpreted the data, and wrote the manuscript. All authors discussed the results and commented on the manuscript.

DECLARATION OF INTERESTS

The authors declare no competing interests.

Received: September 23, 2021
Revised: May 5, 2022
Accepted: June 19, 2022
Published: July 12, 2022

REFERENCES

Aarts, M., Georgilis, A., Beniazza, M., Beolchi, P., Banito, A., Carroll, T., Kulisic, M., Kaemena, D.F., Dharmalingam, G., Martin, N., et al. (2017). Coupling shRNA screens with single-cell RNA-seq identifies a dual role for mTOR in reprogramming-induced senescence. Genes Dev. *31*, 2085–2098. https://doi.org/10.1101/gad.297796.117.

Abad, M., Mosteiro, L., Pantoja, C., Cañamero, M., Rayon, T., Ors, I., Graña, O., Megías, D., Domínguez, O., Martínez, D., et al. (2013). Reprogramming in vivo produces teratomas and iPS cells with totipotency features. Nature *502*, 340–345. https://doi.org/10.1038/nature12586.

Ansieau, S., Bastid, J., Doreau, A., Morel, A.P., Bouchet, B.P., Thomas, C., Fauvet, F., Puisieux, I., Doglioni, C., Piccinin, S., et al. (2008). Induction of EMT by twist proteins as a collateral effect of tumor-promoting inactivation of premature senescence. Cancer Cell *14*, 79–89. https://doi.org/10.1016/j.ccr.2008.06.005.

Banito, A., Rashid, S.T., Acosta, J.C., Li, S., Pereira, C.F., Geti, I., Pinho, S., Silva, J.C., Azuara, V., Walsh, M., et al. (2009). Senescence impairs successful reprogramming to pluripotent stem cells. Genes Dev. *23*, 2134–2139. https://doi.org/10.1101/gad.1811609.

Basisty, N., Kale, A., Jeon, O.H., Kuehnemann, C., Payne, T., Rao, C., Holtz, A., Shah, S., Sharma, V., Ferrucci, L., et al. (2020). A proteomic atlas of senescence-associated secretomes for aging biomarker development. PLoS Biol. *18*, e3000599. https://doi.org/10.1371/journal.pbio.3000599.

Berasain, C., and Avila, M.A. (2014). Amphiregulin. Semin. Cell Dev. Biol. *28*, 31–41. https://doi.org/10.1016/j.semcdb.2014.01.005.

Bindea, G., Mlecnik, B., Hackl, H., Charoentong, P., Tosolini, M., Kirilovsky, A., Fridman, W.H., Pagès, F., Trajanoski, Z., and Galon, J. (2009). ClueGO: a Cytoscape plug-in to decipher functionally grouped gene ontology and pathway annotation networks. Bioinformatics *25*, 1091–1093. https://doi.org/10.1093/bioinformatics/btp101.

Borghesan, M., Fafián-Labora, J., Eleftheriadou, O., Carpintero-Fernández, P., Paez-Ribes, M., Vizcay-Barrena, G., Swisa, A., Kolodkin-Gal, D., Ximénez-Embún, P., Lowe, R., et al. (2019). Small extracellular vesicles are key regulators of non-cell autonomous intercellular communication in senescence via the interferon protein IFITM3. Cell Rep. *27*, 3956–3971.e6. https://doi.org/10.1016/j.celrep.2019.05.095.

Brady, J.J., Li, M., Suthram, S., Jiang, H., Wong, W.H., and Blau, H.M. (2013). Early role for IL-6 signalling during generation of induced pluripotent stem cells revealed by heterokaryon RNA-Seq. Nat. Cell Biol. *15*, 1244–1252. https://doi.org/10.1038/ncb2835.

Burzyn, D., Kuswanto, W., Kolodin, D., Shadrach, J.L., Cerletti, M., Jang, Y., Sefik, E., Tan, T.G., Wagers, A.J., Benoist, C., and Mathis, D. (2013). A special population of regulatory T cells potentiates muscle repair. Cell *155*, 1282–1295. https://doi.org/10.1016/j.cell.2013.10.054.

Chiche, A., Chen, C., and Li, H. (2020). The crosstalk between cellular reprogramming and senescence in aging and regeneration. Exp. Gerontol. *138*, 111005. https://doi.org/10.1016/j.exger.2020.111005.

Chiche, A., Le Roux, I., von Joest, M., Sakai, H., Aguín, S.B., Cazin, C., Salam, R., Fiette, L., Alegria, O., Flamant, P., et al. (2017). Injury-induced senescence enables in vivo reprogramming in skeletal muscle. Cell Stem Cell *20*, 407–414.e4. https://doi.org/10.1016/j.stem.2016.11.020.

Coppé, J.P., Desprez, P.Y., Krtolica, A., and Campisi, J. (2010). The senescence-associated secretory phenotype: the dark side of tumor suppression. Annu. Rev. Pathol. *5*, 99–118. https://doi.org/10.1146/annurev-pathol-121808-102144.

Cox, J., Hein, M.Y., Luber, C.A., Paron, I., Nagaraj, N., and Mann, M. (2014). Accurate proteome-wide label-free quantification by delayed normalization and maximal peptide ratio extraction, termed MaxLFQ. Mol. Cell. Proteomics *13*, 2513–2526. https://doi.org/10.1074/mcp.m113.031591.

Cox, J., and Mann, M. (2008). MaxQuant enables high peptide identification rates, individualized p.p.b.-range mass accuracies and proteome-wide protein quantification. Nat. Biotechnol. *26*, 1367–1372. https://doi.org/10.1038/nbt.1511.

Cox, J., Neuhauser, N., Michalski, A., Scheltema, R.A., Olsen, J.V., and Mann, M. (2011). Andromeda: a peptide search engine integrated into the MaxQuant environment. J. Proteome Res. *10*, 1794–1805. https://doi.org/10.1021/pr101065j.

Demaria, M., Ohtani, N., Youssef, S.A., Rodier, F., Toussaint, W., Mitchell, J.R., Laberge, R.M., Vijg, J., Van Steeg, H., Dollé, M., et al. (2014). An essential role for senescent cells in optimal wound healing through secretion of PDGF-AA. Dev. Cell *31*, 722–733. https://doi.org/10.1016/j.devcel.2014.11.012.

Giai Gianetto, Q., Combes, F., Ramus, C., Bruley, C., Couté, Y., and Burger, T. (2016). Calibration plot for proteomics: a graphical tool to visually check the assumptions underlying FDR control in quantitative experiments. Proteomics *16*, 29–32. https://doi.org/10.1002/pmic.201500189.

Gillet, L.C., Navarro, P., Tate, S., Röst, H., Selevsek, N., Reiter, L., Bonner, R., and Aebersold, R. (2012). Targeted data extraction of the MS/MS spectra generated by data-independent acquisition: a new concept for consistent and accurate proteome analysis. Mol. Cell. Proteomics *11*, O111.016717. https://doi.org/10.1074/mcp.O111.016717.

Herbst, R.S. (2004). Review of epidermal growth factor receptor biology. Int. J. Radiat. Oncol. Biol. Phys. *59*, 21–26. https://doi.org/10.1016/j.ijrobp.2003.11.041.

Hernandez-Segura, A., de Jong, T.V., Melov, S., Guryev, V., Campisi, J., and Demaria, M. (2017). Unmasking transcriptional heterogeneity in senescent cells. Curr. Biol. *27*, 2652–2660.e4. https://doi.org/10.1016/j.cub.2017.07.033.

Hernandez-Segura, A., Nehme, J., and Demaria, M. (2018). Hallmarks of cellular senescence. Trends Cell Biol. *28*, 436–453. https://doi.org/10.1016/j.tcb.2018.02.001.

Hong, H., Takahashi, K., Ichisaka, T., Aoi, T., Kanagawa, O., Nakagawa, M., Okita, K., and Yamanaka, S. (2009). Suppression of induced pluripotent stem cell generation by the p53-p21 pathway. Nature *460*, 1132–1135. https://doi.org/10.1038/nature08235.

Ito, Y., Hoare, M., and Narita, M. (2017). Spatial and temporal control of senescence. Trends Cell Biol. *27*, 820–832. https://doi.org/10.1016/j.tcb.2017.07.004.

Jones, J.T., Akita, R.W., and Sliwkowski, M.X. (1999). Binding specificities and affinities of egf domains for ErbB receptors. FEBS Lett. *447*, 227–231. https://doi.org/10.1016/s0014-5793(99)00283-5.

Kalluri, R., and LeBleu, V.S. (2020). The biology, function, and biomedical applications of exosomes. Science *367*, eaau6977. https://doi.org/10.1126/science.aau6977.

Kawamura, T., Suzuki, J., Wang, Y.V., Menendez, S., Morera, L.B., Raya, A., Wahl, G.M., and Belmonte, J.C.I. (2009). Linking the p53 tumour suppressor pathway to somatic cell reprogramming. Nature *460*, 1140–1144. https://doi.org/10.1038/nature08311.

Kim, C.H., Chae, H.D., Cheon, Y.P., Kang, B.M., Chang, Y.S., and Mok, J.E. (1999). The effect of epidermal growth factor on the preimplantation development, implantation and its receptor expression in mouse embryos. J. Obstet. Gynaecol. Res. *25*, 87–93. https://doi.org/10.1111/j.1447-0756.1999.tb01128.x.

Kopf, M., Baumann, H., Freer, G., Freudenberg, M., Lamers, M., Kishimoto, T., Zinkernagel, R., Bluethmann, H., and Köhler, G. (1994). Impaired immune and acute-phase responses in interleukin-6-deficient mice. Nature *368*, 339–342. https://doi.org/10.1038/368339a0.

Kuilman, T., Michaloglou, C., Vredeveld, L.C., Douma, S., van Doorn, R., Desmet, C.J., Aarden, L.A., Mooi, W.J., and Peeper, D.S. (2008). Oncogene-induced senescence relayed by an interleukin-dependent inflammatory network. Cell *133*, 1019–1031. https://doi.org/10.1016/j.cell.2008.03.039.

Li, H., Collado, M., Villasante, A., Strati, K., Ortega, S., Cañamero, M., Blasco, M.A., and Serrano, M. (2009). The Ink4/Arf locus is a barrier for iPS cell reprogramming. Nature *460*, 1136–1139. https://doi.org/10.1038/nature08290.

Liu, X., Sun, H., Qi, J., Wang, L., He, S., Liu, J., Feng, C., Chen, C., Li, W., Guo, Y., et al. (2013). Sequential introduction of reprogramming factors reveals a time-sensitive requirement for individual factors and a sequential EMT-MET mechanism for optimal reprogramming. Nat. Cell Biol. *15*, 829–838. https://doi.org/10.1038/ncb2765.

Mahmoudi, S., Mancini, E., Xu, L., Moore, A., Jahanbani, F., Hebestreit, K., Srinivasan, R., Li, X., Devarajan, K., Prélot, L., et al. (2019). Heterogeneity in old fibroblasts is linked to variability in reprogramming and wound healing. Nature *574*, 553–558. https://doi.org/10.1038/s41586-019-1658-5.

Mai, T., Markov, G.J., Brady, J.J., Palla, A., Zeng, H., Sebastiano, V., and Blau, H.M. (2018). NKX3-1 is required for induced pluripotent stem cell reprogramming and can replace OCT4 in mouse and human iPSC induction. Nat. Cell Biol. *20*, 900–908. https://doi.org/10.1038/s41556-018-0136-x.

Marion, R.M., Strati, K., Li, H., Tejera, A., Schoeftner, S., Ortega, S., Serrano, M., and Blasco, M.A. (2009). Telomeres acquire embryonic stem cell characteristics in induced pluripotent stem cells. Cell Stem Cell *4*, 141–154. https://doi.org/10.1016/j.stem.2008.12.010.

Mosteiro, L., Pantoja, C., Alcazar, N., Marión, R.M., Chondronasiou, D., Rovira, M., Fernandez-Marcos, P.J., Muñoz-Martin, M., Blanco-Aparicio, C., Pastor, J., et al. (2016). Tissue damage and senescence provide critical signals for cellular reprogramming in vivo. Science *354*, aaf4445. https://doi.org/10.1126/science.aaf4445.

Mosteiro, L., Pantoja, C., de Martino, A., and Serrano, M. (2018). Senescence promotes in vivo reprogramming through p16(INK)(4a) and IL-6. Aging Cell *17*, e12711. https://doi.org/10.1111/acel.12711.

Muñoz-Espín, D., and Serrano, M. (2014). Cellular senescence: from physiology to pathology. Nat. Rev. Mol. Cell Biol. *15*, 482–496. https://doi.org/10.1038/nrm3823.

Ocampo, A., Reddy, P., Martinez-Redondo, P., Platero-Luengo, A., Hatanaka, F., Hishida, T., Li, M., Lam, D., Kurita, M., Beyret, E., et al. (2016). In vivo amelioration of age-associated hallmarks by partial reprogramming. Cell *167*, 1719–1733.e12. https://doi.org/10.1016/j.cell.2016.11.052.

Perez-Riverol, Y., Csordas, A., Bai, J., Bernal-Llinares, M., Hewapathirana, S., Kundu, D.J., Inuganti, A., Griss, J., Mayer, G., Eisenacher, M., et al. (2019). The PRIDE database and related tools and resources in 2019: improving support for quantification data. Nucleic Acids Res. *47*, D442–D450. https://doi.org/10.1093/nar/gky1106.

Pommer, M., Kuphal, S., and Bosserhoff, A.K. (2021). Amphiregulin regulates melanocytic senescence. Cells *10*, 326.

Rhinn, M., Ritschka, B., and Keyes, W.M. (2019). Cellular senescence in development, regeneration and disease. Development *146*, dev151837.

Ritchie, M.E., Phipson, B., Wu, D., Hu, Y., Law, C.W., Shi, W., and Smyth, G.K. (2015). Limma powers differential expression analyses for RNA-sequencing and microarray studies. Nucleic Acids Res. *43*, e47. https://doi.org/10.1093/nar/gkv007.

Robinton, D.A., and Daley, G.Q. (2012). The promise of induced pluripotent stem cells in research and therapy. Nature *18* (*481(7381)*), 295–305. https://doi.org/10.1038/nature10761.

Ruiz, S., Panopoulos, A.D., Herrerías, A., Bissig, K.D., Lutz, M., Berggren, W.T., Verma, I.M., and Izpisua Belmonte, J.C. (2011). A high proliferation rate is required for cell reprogramming and maintenance of human embryonic stem cell identity. Curr. Biol. *21*, 45–52. https://doi.org/10.1016/j.cub.2010.11.049.

Samavarchi-Tehrani, P., Golipour, A., David, L., Sung, H.K., Beyer, T.A., Datti, A., Woltjen, K., Nagy, A., and Wrana, J.L. (2010). Functional genomics reveals a BMP-driven mesenchymal-to-epithelial transition in the initiation of somatic cell reprogramming. Cell Stem Cell *7*, 64–77. https://doi.org/10.1016/j.stem.2010.04.015.

Sancho-Martinez, I., and Belmonte, J.C.I. (2013). Stem cells: surf the waves of reprogramming. Nature *493*, 310–311. https://doi.org/10.1038/493310b.

Schuldiner, M., Yanuka, O., Itskovitz-Eldor, J., Melton, D.A., and Benvenisty, N. (2000). Effects of eight growth factors on the differentiation of cells derived from human embryonic stem cells. Proc. Natl. Acad. Sci. USA *97*, 11307–11312. https://doi.org/10.1073/pnas.97.21.11307.

Serrano, A.L., Baeza-Raja, B., Perdiguero, E., Jardí, M., and Muñoz-Cánoves, P. (2008). Interleukin-6 is an essential regulator of satellite cell-mediated skeletal muscle hypertrophy. Cell Metabol. *7*, 33–44. https://doi.org/10.1016/j.cmet.2007.11.011.

Shiraha, H., Gupta, K., Drabik, K., and Wells, A. (2000). Aging fibroblasts present reduced epidermal growth factor (EGF) responsiveness due to preferential loss of EGF receptors. J. Biol. Chem. *275*, 19343–19351. https://doi.org/10.1074/jbc.m000008200.

Shoyab, M., McDonald, V.L., Bradley, J.G., and Todaro, G.J. (1988). Amphiregulin: a bifunctional growth-modulating glycoprotein produced by the phorbol 12-myristate 13-acetate-treated human breast adenocarcinoma cell line MCF-7. Proc. Natl. Acad. Sci. USA *85*, 6528–6532. https://doi.org/10.1073/pnas.85.17.6528.

Shoyab, M., Plowman, G.D., McDonald, V.L., Bradley, J.G., and Todaro, G.J. (1989). Structure and function of human amphiregulin: a member of the epidermal growth factor family. Science *243*, 1074–1076. https://doi.org/10.1126/science.2466334.

Smyth, G.K. (2005). limma: Linear Models for Microarray Data. Bioinformatics and Computational Biology Solutions Using R and Bioconductor (New York, NY: Springer), pp. 397–420.

Takahashi, K., and Yamanaka, S. (2006). Induction of pluripotent stem cells from mouse embryonic and adult fibroblast cultures by defined factors. Cell *126* (*4*), 663–676. https://doi.org/10.1016/j.cell.2006.07.024.

Thery, C., Amigorena, S., Raposo, G., and Clayton, A. (2006). Isolation and characterization of exosomes from cell culture supernatants and biological fluids. Curr. Protoc. Cell Biol. *3*, 3.22. https://doi.org/10.1002/0471143030.cb0322s30.

Tran, K.T., Rusu, S.D., Satish, L., and Wells, A. (2003). Aging-related attenuation of EGF receptor signaling is mediated in part by increased protein tyrosine

phosphatase activity. Exp. Cell Res. *289*, 359–367. https://doi.org/10.1016/s0014-4827(03)00287-8.

Utikal, J., Polo, J.M., Stadtfeld, M., Maherali, N., Kulalert, W., Walsh, R.M., Khalil, A., Rheinwald, J.G., and Hochedlinger, K. (2009). Immortalization eliminates a roadblock during cellular reprogramming into iPS cells. Nature *460*, 1145–1148. https://doi.org/10.1038/nature08285.

Wieczorek, S., Combes, F., Lazar, C., Giai Gianetto, Q., Gatto, L., Dorffer, A., Hesse, A.M., Couté, Y., Ferro, M., Bruley, C., and Burger, T. (2017). DAPAR & ProStaR: software to perform statistical analyses in quantitative discovery proteomics. Bioinformatics *33*, 135–136. https://doi.org/10.1093/bioinformatics/btw580.

Wood, E.R., Truesdale, A.T., McDonald, O.B., Yuan, D., Hassell, A., Dickerson, S.H., Ellis, B., Pennisi, C., Horne, E., Lackey, K., et al. (2004). A unique structure for epidermal growth factor receptor bound to GW572016 (Lapatinib): relationships among protein conformation, inhibitor off-rate, and receptor activity in tumor cells. Cancer Res. *64*, 6652–6659. https://doi.org/10.1158/0008-5472.can-04-1168.

Xu, Q., Long, Q., Zhu, D., Fu, D., Zhang, B., Han, L., Qian, M., Guo, J., Xu, J., Cao, L., et al. (2019). Targeting amphiregulin (AREG) derived from senescent stromal cells diminishes cancer resistance and averts programmed cell death 1 ligand (PD-L1)-mediated immunosuppression. Aging Cell *18*, e13027. https://doi.org/10.1111/acel.13027.

Yu, M., Wei, Y., Xu, K., Liu, S., Ma, L., Pei, Y., Hu, Y., Liu, Z., Zhang, X., Wang, B., et al. (2019). EGFR deficiency leads to impaired self-renewal and pluripotency of mouse embryonic stem cells. PeerJ *7*, e6314. https://doi.org/10.7717/peerj.6314.

Yuan, J.S., Reed, A., Chen, F., and Stewart, C.N., Jr. (2006). Statistical analysis of real-time PCR data. BMC Bioinf. *7*, 85. https://doi.org/10.1186/1471-2105-7-85.

Yun, M.H., Davaapil, H., and Brockes, J.P. (2015). Recurrent turnover of senescent cells during regeneration of a complex structure. Elife *4*, e05505. https://doi.org/10.7554/elife.05505.

Zaiss, D.M.W., Gause, W.C., Osborne, L.C., and Artis, D. (2015). Emerging functions of amphiregulin in orchestrating immunity, inflammation, and tissue repair. Immunity *42*, 216–226. https://doi.org/10.1016/j.immuni.2015.01.020.

Zhang, C., Li, Y., Wu, Y., Wang, L., Wang, X., and Du, J. (2013). Interleukin-6/signal transducer and activator of transcription 3 (STAT3) pathway is essential for macrophage infiltration and myoblast proliferation during muscle regeneration. J. Biol. Chem. *288*, 1489–1499. https://doi.org/10.1074/jbc.m112.419788.

STAR★METHODS

KEY RESOURCES TABLE

REAGENT or RESOURCE	SOURCE	IDENTIFIER
Antibodies		
Rat anti-IL6 (clone MP5-20F3)	eBiosciences	Cat#14-7061-85; RRID: AB_468423
Rat IgG1 control (clone RTK2071)	BioLegend	Cat#400402; RRID: AB_326508
Rabbit anti-Nanog (Homemade) (Clone H22)	Crb	N/A
Chemicals, peptides, and recombinant proteins		
Recombinant mouse AREG	R&D system	Cat# 989-AR-100
Recombinant human AREG	R&D system	Cat# 262-AR-100
EGF	R&D	Cat# 2028-EGF
Lapatinib	Tebu-Bio	Cat# T0078
polyethylenimine, linear, MW25000	polysciences Europe	Cat# 23966-100mg
KSR	Invitrogen	Cat# 10828028
LIF	Miltenyl Biotec	Cat# 130-09
Poly-L-Lysine	Sigma	Cat# P4707
Snake venom cardiotoxin	Merck Chimie SAS	Cat# 217503
X-gal	Euromedex	Cat# EU0012
Critical commercial assays		
Alkaline phosphatase activity	Sigma	Cat# AB0300
LightCycler 480 SYBR Green I Master	Roche	Cat# 04887352001
Experimental models: Cell lines		
Human BJ fibroblast	Li et al., 2009	N/A
Experimental models: Organisms/strains		
Mouse: i4F	Abad et al., 2013	N/A
Mouse: IL6 -/-	Kopf et al., 1994	N/A
Oligonucleotides		
qPCR primers	Sigma	Table S4
Recombinant DNA		
pbabe-hRASV12-puro	Addgene	Cat# 9051
pbabe-puro	Addgene	Cat# 1764
pMXs-hKlf4, pMXs-hSox2, pMXs-hOct4 and pMXs-hc-Myc	Addgene	Cat# 17217-20
Software and algorithms		
ImageJ software		https://imagej.nih.gov/ij/download.html
FlowJo software		https://www.flowjo.com
Graphpad		Prism software
Sendetect	This paper	N/A
Other		
Proteomic data	This paper	ProteomeXchange via the PRIDE database (PXD028590)
Original Western Blot image	This paper	https://doi.org/10.17632/nk77w7pkvw.1

RESOURCE AVAILABILITY

Lead contact

Further information and requests for resources and reagents should be directed to and will be fulfilled by the lead contact, Han Li (han.li@pasteur.fr).

Materials availability

This study did not generate new unique reagents.

Data and code availability

The proteomic data has been deposited at the ProteomeXchange via the PRIDE database and are publicly available as of the date of publication. Accession numbers are listed in the key resources table. Original western blot images have been deposited at Mendeley and are publicly available as of the date of publication. The DOI is listed in the key resources table.

Any additional information required to reanalyze the data reported in this paper is available from the lead contact upon request.

EXPERIMENTAL MODELS AND SUBJECT DETAILS

Mice and breeding

Animals were handled as per European Community guidelines and the ethics committee of the Institut Pasteur (CETEA) approved protocols. The reprogrammable i4F mice were kindly provided by Manuel Serrano (Spanish National Cancer Research Centre, Madrid, Spain) (Abad et al., 2013). The $Il6^{-/-}$ were described previously (Kopf et al., 1994) and were crossed with i4F. To induce muscle injury, mice were anesthetized with isoflurane. *Tibialis anterior* (TA) muscles were injured by injection 50μl of snake venom cardiotoxin (10μM) (Merck, 217503). *In vivo* reprogramming was induced by administration of Doxycycline (Sigma) in the drinking water supplemented with 7.5% of sucrose right after injury. Experiments were performed indistinguishably with male mice from 6 to 8 weeks of age except indicated otherwise.

METHOD DETAILS

Animal procedures

For recombinant AREG injection, after muscle injury by cardiotoxin, mice were intraperitoneally injected by AREG (989-AR, R&D systems) or PBS control at the concentration of 7 μg/mouse at days 2, 4, 6 and 8-post injury and TAs were collects at 10 days-post injury. The initial AREG injection was done intra-muscularly (1ug/TA).

Cell culture conditions

Primary mouse embryo fibroblasts (MEFs, passage 2) were obtained from pure inbred C57BL6 background WT or reprogrammable mice, as described previously (Li et al., 2009). Mouse dermal fibroblasts (MDFs) were obtained from the ear of young (2 months) and old (2 years) i4F mice as described before (Li et al., 2009). Fibroblasts (MEFs and MDFs) were cultured in standard DMEM medium with 10% FBS (Gibco) and 1% Pen/Strep (Gibco).

Induction of senescence

γ-irradiation induced senescence (IRIS): WT MEFs were treated with ionizing radiation (10 Gy X-ray). Quiescent control cells were mock irradiated. Oncogene Induced Senescence (OIS): MEFs were infected with hRAS viral particles or control vector particles. Following infection, cells were selected with puromycin (gene resistance marker) for 4 days and seeded at proper density on tissue culture plates previously treated with gelatin 0.1% (10 min at RT) for further experiments. Replicative Senescence (RS): MEFs were propagated every 3 days under 3% O_2 (physiological condition) or 20% O_2 with 5% CO_2. Cells were seeded at 20% confluency and passed upon reaching 80–90% confluency. This protocol was performed until cells reached replicative crisis and they stopped growing. Then cells were seeded at proper density on tissue culture plates previously treated with gelatin 0,1% for further experiments. Media was changed every 2 days. Senescent cells were cultured for 10 days to allow development of the senescent phenotype, and quiescent cells were cultured in 0.2% serum for 3 days.

Collection of CM

Senescent cells were then washed with PBS (Thermo Fisher Scientific) and placed in serum- and phenol red–free DMEM (Thermo Fisher Scientific, Waltham, MA; #21063–029), and conditioned media was collected after 48 h and filtered through 0.2μm filter.

Soluble fraction and sEV isolation

Whole CM was centrifuged at 500g for 10min filtered through 0.2μm filter unit. Next, filtered CM was centrifuged at 12 000g for 30 min at 4°C, pellet was removed, and supernatant was centrifuged at 100 000g for 3 h to collect the soluble fraction (SN) absence of exosome. The pellet was resuspended with PBS and centrifuged at 100 000g for additional 3 h. The purified pellets were collected and resuspended into proper medium for further experiments without further concentration. Samples were centrifuged using an Ultracentrifuge Optima XPN-80 Ultracentrifuge from Beckman Coulter equipped with a rotor SW32Ti.

In vitro reprogramming in co-culture & CM system

For the co-culture system, primary i4F MEFs were seeded over senescent or quiescent cells described above at density of $2x10^4$ per well in 6-well plate. For conditioned medium system, primary i4F MEFs were seeded at the density of $5x10^3$ per well in 6-well plate.

In vitro reprogramming was induced on the second day by changing to the iPSCs medium of high-glucose DMEM supplemented with KSR (15%, Invitrogen), LIF (1,000 U/ml), non-essential amino acids, penicillin-streptomycin, glutamax and β-mercaptoethanol) supplement with doxycycline (1 μg/ml) as described previously (Abad et al., 2013). For the CM system, conditioned medium from either senescent or quiescent cells were used instead of high-glucose DMEM and the rest components were added as described above. Medium was changed every 48h until iPS cell colonies appeared. Reprogramming of human BJ cells was performed as described previously (Li et al., 2009). Briefly, BJ fibroblasts had been seeded (2×10^5 cells per well in 6-well gelatin-coated plates) the day before the infection. The infection was repeated every 12h for 2 days. The day after infection was completed, medium was replaced, and kept for three more days. At day 5, cells were trypsinized and reseeded on feeder plates. At day 6, medium was changed to human ES cell medium. Cultures were maintained in the absence of drug selection with daily medium changes. For the IL-6 blocking antibody experiment, IgG antibody (1μg/mL, BioLegend, purified Rat IgG1, κ Isotype Ctrl Antibody) and anti-IL-6 antibody (3μg/mL, eBioscience clone MP5-20F3) were used. For AREG, EGF, and Lapatinib experiment, mouse AREG (200ng/ml excepted indicated otherwise, R&D Systems, 989-AR), human AREG (200ng/ml, Bio-Techne, 262-AR-100), EGF (R&D Systems, 2028-EG), and Lapatinib (Tebu-Bio, T0078) were used for the first three days. Medium were changed every 24h until iPS colonies appeared. PBS were used as the control. Reprogramming plates were stained for alkaline phosphatase activity (Sigma, AP detection kit AB0300) and quantified using ImageJ software.

For the proliferation analysis, $2x10^3$ cells of primary i4F MEFs were seeded in triplicates onto wells of 12-well plates. Cell number were counted using Neubauer chamber every two days for 10–12 days period. Medium were changed every 24h.

Plasmids and infections

Retroviral vectors pbabe-hRASV12-puro (Addgene #9051) and pbabe-puro (Addgene #1764) (control) were used for infections of MEFs to induce senescence. Following day after infection, cells were selected with puromycin (4μg/mL) (Sigma, P8833). Retroviral vectors pMXs-hKlf4, pMXs-hSox2, pMXs-hOct4 and pMXs-hc-Myc (Addgene #17217-20) were used for infect human BJ fibroblasts for reprogramming together with ecotropic packaging plasmid pCL-Ampho. HEK 293 cells were transfected using PEI (Polyethylenimine) with a 1:4 ratio of DNA:PEI. MEFs were infected twice per day for 2 days (12h interval). Viral supernatant was collected, centrifuged at 300g, and filtered through 0,45μm. Polybrene was used (8μg/mL) (Sigma, TR-1003).

Proteomic sample preparation

Chemicals

Acetonitrile (ACN, #412342) was from Carlo Erba, Iodoacetamide ((#I114), Tris(2-carboxyethyl)phosphine hydrochloride (TCEP, #646547), Trichloroacetic acid (TCA, #T6399), ammonium bicarbonate (#09830) were from Sigma-Aldrich (USA), formic acid (#94318, Fluka), Urea (#29700) was from Thermo Scientific (Waltham, MA), sequencing grade trypsin (#V5111) was from Promega (San Luis Obispo, CA), and Sep-Pak C18 cartridge (50mg sorbent, #WAT054955) were from Waters (Milford, USA).

Sample collection

OIS and mock-infected cells were washed with DMEM twice before incubation with DMEM (without FBS and Pen/Strep) for 48 h at 37°C under normal conditions. CM was collected, centrifuged 10 min at 500g, filtered through 0,2μm filter unit and centrifuged at 12 000g for 30 min at 4°C. Pellets (containing sEVs) were removed. CM was centrifuged for additional 3 h at 100 000g. CM was kept frozen for further analysis.

Digestions

Two technical replicates were processed for every sample. Proteins from the secretome were precipitated 1hour at 4°C with TCA (20%) and centrifugated 15min at 16 000g in 4°C. The pellets were washed twice with ice-cold acetone and resuspended in denaturation buffer containing 8M Urea/100mM ammonium bicarbonate. The mixtures were reduced with 50mM TCEP (37°C for 1 h), then alkylated with 50 mM iodoacetamide (1 h at RT in the dark). Samples were diluted 9-fold with 100mM ammonium bicarbonate and incubated overnight at 37°C with sequencing grade modified trypsin (Promega, San Luis Obispo, CA) at a 1:40 enzyme: substrate ratio (wt/wt).

Desalting

4% FA was added to stop the reaction. Digested peptides were purified with Sep-Pak C18 and were eluted with 80% ACN containing 0.1% formic acid in water. Resulting peptides were dried and resuspended in 2% ACN containing 0.1% formic acid in water.

Mass spectrometry analysis

Samples acquisitions were performed on a Q Exactive™ Plus Mass Spectrometer (Thermo Fisher Scientific, USA) coupled with a Proxeon EASY-nLC 1200 (Thermo Fisher Scientific, USA). 1μg of peptides were injected onto a home-made 55 cm C18 column (1.9 μm particles, 100 Å pore size, ReproSil-Pur Basic C18, Dr. Maisch GmbH, Ammerbuch-Entringen, Germany) and eluted with a multi-step gradient, using buffer A (0.1% FA) and buffer B (80% ACN), from 2 to 7% buffer B in 5min, 7% to 23% buffer B in 70min, 23 to 45% buffer B in 30min and 45 to 95% buffer B in 5min, at a flow rate of 250 nL/min over 132 min. The column temperature was set to 60°C.

MS data were acquired using Xcalibur software using a data-dependent method. MS scans were acquired at a resolution of 70,000 and MS/MS scans (fixed first mass 100 m/z) at a resolution of 17,500. The AGC target and maximum injection time for the survey scans and the MS/MS scans were set to 3E6, 20ms, and 1E6, 60ms, respectively. An automatic selection of the 10 most intense precursor ions was activated (Top 10) with a 45s dynamic exclusion. The isolation window was set to 1.6 m/z and normalized collision

energy fixed to 28 for HCD fragmentation. We used an underfill ratio of 1E4 for an intensity threshold of 1.7E5. Unassigned precursor ion charge states as well as 1, 7, 8, and >8 charged states were rejected, and peptide match was disable.

Processing, quantification, and statistical analysis of MS data

Raw data were analyzed using MaxQuant software version 1.5.5.1 (Cox and Mann, 2008) using the Andromeda search engine (Cox et al., 2011). The MS/MS spectra were searched against the mus musculus SwissProt database (53.449 entries from UniProt the 24/07/2018). Variable modifications (methionine oxidation, N-terminal acetylation) and fixed modification (cysteine carbamidomethylation) were set for the search and trypsin with a maximum of two missed cleavages was chosen for searching. The minimum peptide length was set to 7 amino acids and the false discovery rate (FDR) for peptide and protein identification was set to 0.01. At least a unique peptide per protein group was required for the identification of protein. The main search peptide tolerance was set to 4.5 ppm and to 20 ppm for the MS/MS match tolerance. Second peptides were enabled to identify co-fragmentation events. Match between runs option was selected with a match time window of 0.7 min and an alignment time window of 20 min for biological replicates of a same condition. Quantification was performed using the XIC-based LFQ algorithm with the Fast LFQ mode as previously described (Cox et al., 2014). Unique and razor peptides, included modified peptides, with at least 2 ratio counts were accepted for quantification. For the differential analyses, reverses, potential contaminants and ''only identified by site'' proteins were first discarded from the list of identified proteins. Then, only proteins with at least 6 LFQ values in a condition were kept. After log2 transformation, LFQ values were normalized by median centering within conditions (wrapper.normalize D function of the R package DAPAR) (Wieczorek et al., 2017). Exclusive proteins that are present in only one condition were grouped and isolated as ''differentially abundant proteins''. Next, missing values were imputed using the imp.norm function of the R package *norm* of Novo (2013). Proteins with a fold-change under 2.0 were considered not differentially abundant. Statistical testing of the remaining proteins (having a fold-change over 2.0) was conducted using a limma t-test (Smyth, 2005) thanks to the R package *limma* (Ritchie et al., 2015). An adaptive Benjamini-Hochberg procedure was applied on the resulting p-values thanks to the function adjust.p of R package *cp4p* (Giai Gianetto et al., 2016) to estimate the proportion of true null hypotheses among the set of statistical tests. The proteins associated to an adjusted p-value inferior to an FDR of 1% were considered as differentially abundant proteins. The mass spectrometry proteomics data have been deposited to the ProteomeXchange Consortium via the PRIDE partner repository with the dataset identifier PXD (Perez-Riverol et al., 2019).

Pathway and network analysis

Gene ontology, pathway, and network analysis was performed using the GlueGO package, version 2.5.3, in Cytoscape (https://cytoscape.org/), version 3.7.1 [33,34]. Curated pathways for enrichment analysis were referenced from the database of GO Biological Process. For gene ontology data, testing was restricted to pathways with experimental evidence (EXP, IDA, IPI, IMP, IGI, IEP). The statistical cutoff for enriched pathways was Bonferroni-adjusted p-values <0.01 by right-sided hypergeometric testing. Pathway-connecting edges were drawn for kappa scores >40%. Kappa scores are a measure of inter-pathway agreement among observed proteins that indicate whether pathway agreement is greater than expected by chance based on shared proteins. Pathways with the same color indicate $\geq$50% similarity in terms. Pathway and network visualizations were generated and modified using the GlueGO package in Cytoscape.

Immunohistochemistry and immunofluorescence

TA muscles were isolated from mice and frozen directly in liquid nitrogen in cooled isopentane (320404, Sigma) for 40 s and Liver, pancreas, kidney and teratoma were imbedded in tissue freezing medium (14020108926, Leica), frozen in cooled isopentane on dry ice, all samples were stored at -80°C or directly cryosectioned in 10-μm sections.

For histology, sections were air dried and fixed with 4% PFA in PBS and washed, then stained with Hematoxylin and Eosin (H&E). For immunohistochemistry, the following primary antibodies were used: anti-Nanog (2ug/ml, H22, produced by Cambridge Research Biochemicals (Crb)). Slides were then incubated with the corresponding secondary antibodies conjugated with peroxidase from Dako (K4003).

SAβGalactosidase (SAβGal) assay

The assay was performed as previously described (Chiche et al., 2017). Briefly, sections were fixed at room temperature for 10 min in a solution containing 2% paraformaldehyde and 0.2% glutaraldehyde in PBS. Sections were washed in PBS and then incubated in an X-gal solution containing 4mM $K3Fe(CN)_6$, 4 mM $K4Fe(CN)_6$, 2 mM MgCl2, 0.02% NP-40 (Igepal) and 1mg/ml X-gal (EU0012, EUROMEDEX) in PBS pH = 5.5) at 37°C for 48 h. X-gal solution was changed after 24h. Samples were washed in PBS and post-fixed in 4% PFA in PBS for 15 min. After washes, samples were counterstained with Fast-red (H3403, VECTOR) and mounted in Eukitt (03989, Sigma). Finally, the sections were scanned using OLYPMPUS VS120, and SAβgal positive cells were quantified using self-developed program ''Sendetect''.

BrdU immunofluorescence staining

Cells were seeded on coverslip coated with Poly-L-Lysine (Sigma) in 24-well plates for analyses. Cells were incubated under different conditions for 72 h then incubated for 1 h with BrdU (10μM). Cells were washed with PBS and fixed in cold 70% EtOH (- 20°C) for 20 min. Cells were washed with PBS and incubated with fresh 2N HCl for 20 min to denature DNA. Cells were washed 3 times with PBS and blocked into 3% BSA blocking solution for 30 min. After blocking cells were incubated with primary antibody for 2 h at RT into humid chamber. Cells were washed with PBS three times prior incubation with secondary antibody for 45 min at RT. Finally, cells were mounted into DAPI Gold antifade mounting medium (Invitrogen, P36931). Images were acquired with an Olympus IX83 microscope and quantified using ImageJ software.

Cell cycle analysis

MEFs were incubated under different conditions. Briefly cells were incubated with BrdU (10μM) for 1h30 min then washed three times with PBS. Cells were collected and were washed with PBS, centrifuged and fixed in cold 70% EtOH. Cells were kept at -20°C until analysis. The day of analysis, fixed cells were centrifuged. Cells were washed with PBS and incubated with fresh 2N HCl for 20 min at RT. Cells were washed and incubated with FITC BrdU antibody (BD Pharmingen, 51-33284X) for 45 min at RT. Cells were washed with PBS, and resuspended in PBS containing Rnase A (100μg/mL) (Qiagen) and Propidium Iodide (50μg/mL) (Sigma Aldrich, P4864). Samples were analyzed at least 2 h after using a Cytoflex Flow Cytometer (Beckman Coulter).

Western Blot

i4F MEFs were seeded on p60 plate and incubated under different conditions. Cells were collected at the indicated different time-points directly in a mix composed of RIPA buffer (Sigma, R0278), DTT, Protease inhibitor cocktail (Sigma, 539131) and phosphatase inhibitor cocktail (Millipore, 524625). Samples were boiled for 5 min at 95°C before loading on polyacrylamide gels. Transfer occurred at 100V for 1hr on nitrocellulose membranes (BioRad). Membranes were blotted with TBST (0.2% Tween) and 5% BSA (Sigma, A3608) and incubated overnight with the primary antibody and for 45min with HRP-conjugated secondary antibody. Bands were revealed with Pierce ECL chemiluminescent substrate (Thermo Scientific, 32109) and analyzed using a ChemiDoc MP (BioRad).

Quantitative real-time PCR

Total RNA was extracted from cells and tissue samples with Trizol (Invitrogen, 15596026) following provider's recommendations, samples were treated with DNase I before reverse transcription into cDNA following the manufacturer's protocol (Applied Biosystems, 4368813). Quantitative real-time PCR was performed using a LightCycler 480 (Roche) using SYBR Green Master (Roche). All values were obtained at least in duplicate, and in a total of at least two independent assays. Calculation for the values was made using the ΔΔCt method, as previously described (Yuan et al., 2006).

QUANTIFICATION AND STATISTICAL ANALYSIS

The number of independent experimental replications, the definition of center and precisions measures are reported in the figure legends (n, mean ± sem or n, mean ± sd). Statistical analyses were performed using the GraphPad Prism v9 software. Statistical significance was assessed by the Mann-Whitney test and ordinary one-way ANOVA. p-value < 0.05 was considered as statistically significant.